Kivijärvi, Ville; Nyman, Markus; Shevchenko, Andriy; Kaivola, Matti

Optical-image transfer through a diffraction-compensating metamaterial

Published in:
Optics Express

DOI:
10.1364/OE.24.009806

Published: 02/05/2016

Document Version
Publisher's PDF, also known as Version of record

Please cite the original version:
Kivijärvi, V., Nyman, M., Shevchenko, A., & Kaivola, M. (2016). Optical-image transfer through a diffraction-compensating metamaterial. *Optics Express*, *24*(9), 9806-9815. https://doi.org/10.1364/OE.24.009806

Optical-image transfer through a diffraction-compensating metamaterial

Ville Kivijärvi, Markus Nyman, Andriy Shevchenko,* and Matti Kaivola

Department of Applied Physics, Aalto University, P.O Box 13500, FI-00076, Aalto, Finland

**andriy.shevchenko@aalto.fi*

Abstract: Cancellation of optical diffraction is an intriguing phenomenon enabling optical fields to preserve their transverse intensity profiles upon propagation. In this work, we introduce a metamaterial design that exhibits this phenomenon for three-dimensional optical beams. As an advantage over other diffraction-compensating materials, our metamaterial is impedance-matched to glass, which suppresses optical reflection at the glass-metamaterial interface. The material is designed for beams formed by TM-polarized plane-wave components. We show, however, that unpolarized optical images with arbitrary shapes can be transferred over remarkable distances in the material without distortion. We foresee multiple applications of our results in integrated optics and optical imaging.

OCIS codes: (160.4236) Nanomaterials; (160.3918) Metamaterials; (050.6624) Subwavelength structures; (050.1940) Diffraction; (350.5500) Propagation.

References and links

1. H. Ghaemi, Y. Tineke, and T. Wang, "Fiber image guide with subwavelength resolution," Appl. Phys. Lett. **72**(10), 1137-1139 (1998).
2. T. Muldoon, M. Pierce, D. Nida, M. Williams, A. Gillenwater, and R. Richards-Kortum, "Subcellular-resolution molecular imaging within living tissue by fiber microendoscopy," Opt. Express **15**(25), 16413 (2007).
3. K. Kempa, X. Wang, Z. Ren, and M. Naughton, "Discretely guided electromagnetic effective medium," Appl. Phys. Lett. **92**(4), 043114 (2008).
4. T. Cizmar and K. Dholakia, "Exploiting multimode waveguides for pure fibre-based imaging," Nat. Commun. **3**, 1027 (2012).
5. S. Karbasi, R. Frazier, K. Koch, T. Hawkins, J. Ballato, and A. Mafi, "Image transport through a disordered optical fibre mediated by transverse Anderson localization," Nat. Commun. **5**, 3362 (2014).
6. H. Kosaka, T. Kawashima, A. Tomita, M. Notomi, T. Tamamura, T. Sato, and S. Kawakami, "Self-collimating phenomena in photonic crystals," Appl. Phys. Lett. **74**(9), 1212-1214 (1999).
7. J. Witzens, M. Lončar, and A. Scherer, "Self-collimation in planar photonic crystals," IEEE J. Sel. Topics Quantum Electron. **8**(6), 1246-1257 (2002).
8. R. Iliew, C. Etrich, and F. Lederer, "Self-collimation of light in three-dimensional photonic crystals," Opt. Express **13**(18), 7076-7085 (2005).
9. J. Shin and S. Fan, "Conditions for self-collimation in three-dimensional photonic crystals," Opt. Lett. **30**(18), 2397-2399 (2005).
10. Z. Lu, S. Shi, J. Murakowski, G. Schneider, C. Schuetz, and D. Prather, "Experimental demonstration of self-collimation inside a three-dimensional photonic crystal," Phys. Rev. Lett. **96**(17), 173902 (2006).
11. D. Prather, S. Shi, J. Murakowski, G. Schneider, A. Sharkawy, C. Chen, B. Miao, and R. Martin, "Self-collimation in photonic crystal structures: a new paradigm for applications and device development," J. Phys. D. Appl. Phys. **40**(9), 2635-2651 (2007).
12. A. Matthews, S. Morrison, and Y. Kivshar, "Self-collimation and beam splitting in low-index photonic crystals," Opt. Commun. **279**(2), 313-319 (2007).
13. W. Park, "Controlling the flow of light with silicon nanostructures," Laser Phys. Lett. **7**(2), 93-103 (2010).

#260019 Received 25 Feb 2016; revised 4 Apr 2016; accepted 22 Apr 2016; published 27 Apr 2016

14. B. Casse, W. Lu, Y. Huang, E. Gultepe, L. Menon, and S. Sridhar, "Super-resolution imaging using three-dimensional metamaterials nanolens," Appl. Phys. Lett. **96**(2), 023114 (2010).
15. Y. Chuang and T. Suleski, "Photonic crystals for broadband, omnidirectional self-collimation," J. Opt. **13**(3), 035103 (2011).
16. J. Arlandis, E. Centero, R. Polles, A. Moreau, and J. Campos, "Mesoscopic self-collimation and slow light in all-positive index layered photonic crystals," Phys. Rev. Lett. **108**(3), 037401 (2012).
17. R. Rumpf, J. Pazos, C. Garcia, L. Ochoa, and R. Wicker, "3D printed lattices with spatially variant self-collimation," Prog. Electromagn. Res. **139**, 1-14 (2013).
18. J. Yao, Z. Liu, Y. Liu, Y. Wang, C. Sun, G. Bartal, A. Stacy, and X. Zhang, "Optical negative refraction in bulk metamaterials of nanowires," Science **321**(5891), 930 (2008).
19. P. Belov, Y. Shao, S. Tse, P. Ikonen, M. Silveirinha, C. Simovski, S. Tretyakov, Y. Hao, and C. Parini, "Transmission of images with subwavelength resolution to distances of several wavelengths in the microwave range," Phys. Rev. B **77**(19), 193108 (2008).
20. T. Paul, C. Rockstuhl, C. Menzel, and F. Lederer, "Anomalous refraction, diffraction, and imaging in metamaterials," Phys. Rev. B **79**(11), 115430 (2009).
21. T. Paul, C. Menzel, C. Rockstuhl, and F. Lederer, "Advanced optical metamaterials," Adv. Mater. **22**(21), 2354-2357 (2010).
22. V. Kivijärvi, M. Nyman, A. Shevchenko, and M. Kaivola, "An optical metamaterial with simultaneously suppressed optical diffraction and surface reflection," J. Opt. **18**(3), 035103 (2016).
23. B. Wood and J. Pendry, "Directed subwavelength imaging using a layered metal-dielectric system," Phys. Rev. B **74**(11), 115116 (2006).
24. Y. Chuang and T. Suleski, "Complex rhombus lattice photonic crystals for broadband all-angle self-collimation," J. Opt. **12**(3), 035102 (2010).
25. D. Zhao, C. Zhou, Q. Gong, and X. Jiang, "Lasing cavities and ultra-fast switch based on self-collimation of photonic crystals," J. Phys. D: Appl. Phys. **41**(11), 115108 (2008).
26. N. Yogesh and V. Subramanian, "Analysis of self-collimation based cavity resonator formed by photonic crystal," Prog. Electromagn. Res. M **12**, 115-130 (2010).
27. C. Menzel, C. Rockstuhl, T. Paul, and F. Lederer, "Retrieving effective parameters for metamaterials at oblique incidence," Phys. Rev. B **77**(19), 195328 (2008).
28. T. Paul, C. Menzel, W. Smigaj, C. Rockstuhl, P. Lalanne, and F. Lederer, "Reflection and transmission of light at periodic layered metamaterial films," Phys. Rev. B **84**(11), 115142 (2011).
29. P. Grahn, A. Shevchenko, and M. Kaivola, "Interferometric description of optical metamaterials," New J. Phys. **15**(6432), 113044 (2013).
30. P. Grahn, A. Shevchenko, and M. Kaivola, "Theoretical description of bifacial optical nanomaterials," Opt. Express **21**(20), 23471 (2013).
31. A. Shevchenko, P. Grahn, and M. Kaivola, "Internally twisted spatially dispersive optical metamaterials," J. Nanophotonics **8**(1), 083074 (2014).
32. A. Shevchenko, V. Kivijärvi, P. Grahn, M. Kaivola, and K. Lindfors, "Bifacial metasurface with quadrupole optical response," Phys. Rev. Appl. **4**(2), 024019 (2015).
33. J. Stratton, *Electromagnetic Theory* (McGraw-Hill, 1941).
34. V. Kivijärvi, M. Nyman, A. Karrila, P. Grahn, A. Shevchenko, and M. Kaivola, "Interaction of optical beams with metamaterials," New J. Phys. **17**(6), 063019 (2015).
35. L. Novotny and B. Hecht, *Principles of Nano-Optics* (Cambridge University, 2006).
36. P. Johnson and R. Christy, "Optical constants of noble metals," Phys. Rev. B. **6**(12), 4370-4379 (1972).

1. Introduction

Due to diffraction, transversely confined optical fields diverge upon propagation in free space. As a result, optical images are not propagation-invariant and can be made sharp only in a single transverse plane. A simple way to overcome the divergence is to guide light in a waveguide such as an optical fiber. As an example, a bundle of optical waveguides can be used to transfer two-dimensional images over long distances without considerable distortions [1–5]. However, the image at the output is usually broken into circular pixels and has a low resolution. A different approach has been proposed in the field of spatially dispersive photonic crystals. It has been shown that, if at a given frequency the wave vector $\mathbf{k}$ in the crystal depends on the wave propagation direction such that its projection onto a certain direction ($\mathbf{z}$) remains constant ($k_z = C$), light will propagate along this direction without divergence [6–17]. The phenomenon is called self-collimation. It is as a rule obtained at a wavelength (λ) close to the Bragg diffraction regime, and therefore, the surface reflectivity of the crystal appears to be high. In addition to

#260019 Received 25 Feb 2016; revised 4 Apr 2016; accepted 22 Apr 2016; published 27 Apr 2016

photonic crystals, hyperbolic-type metamaterials have been shown to exhibit diffraction cancellation [14, 18, 19]. These materials are composed of infinitely wide metal plates or infinitely long metal rods distributed periodically with a period $\Lambda < \lambda/2$. The materials are also spatially dispersive, but for them the condition $k_z = C$ can cover also free-space evanescent waves, which yields subdiffraction-limited resolution for optical-image transfer through the material. The phenomenon is called canalization. Also fishnet metamaterials have been shown to provide diffraction compensation at optical frequencies [20, 21]. These materials, however, show a very high absorption: $\mathrm{Im}(k_z) \approx 6\ \mu\mathrm{m}^{-1}$ corresponding to an imaginary refractive index of ca. 0.7. Recently, we have proposed one more way to suppress optical diffraction by combining spatial dispersion with optical anisotropy of silver-disc metamolecules [22]. Our approach makes it possible to tune the value of the wave impedance in the material towards that of the surrounding medium and, as a result, dramatically reduce the reflection of the metamaterial surface. Often, the materials proposed for diffraction-free guidance of optical beams are two-dimensional, meaning that the beam divergence is suppressed only for waves with wave vectors in a single plane. Materials like these are usually fabricated in the form of a slab waveguide parallel to the plane in question. Waves propagating at an angle to this plane are confined in the slab by total internal reflection.

In this work, we introduce a three-dimensional metamaterial that suppresses optical diffraction for three-dimensional optical fields. The material is composed of silver nanobars aligned parallel to the desired diffraction-compensation axis $\mathbf{z}$. The increase of the wavenumber with the angle θ between $\mathbf{z}$ and $\mathbf{k}$ (required to obtain constant k_z) is achieved for TM polarized waves as a result of their more efficient coupling to the longitudinal plasmon resonance of the nanobars at larger propagation angles θ. We demonstrate the effect of suppressed diffraction with an example of a radially polarized hollow optical beam. Then we consider the possibility to achieve distortion-free transfer of arbitrary two-dimensional images through the designed metamaterial. We show that, if the image is formed by unpolarized or circularly polarized light, it can be transferred through the material without distortion over a remarkable distance, even though the material is designed to deal only with TM-polarized waves. Eventually, the image becomes composed purely of TM-polarized waves, as the TE-polarized part of the image freely spreads in the material. Hence, the material acts as an unconventional optical polarizer. The wave parameters and the wavelength of the diffraction-cancellation effect can be selected by tuning the dimensions of the nanobars and the unit cells. Compared to already demonstrated diffraction-compensating photonic crystals [8–11, 14, 15, 17] and metamaterials [14, 18, 19, 23], our material has a negligible surface reflectivity. In addition, it has a much lower absorption coefficient than typical "canalizing" metamaterials have.

The introduced diffraction-compensating metamaterial can be used as an optical waveguide or a distortion-free image-transferring device. Independently of the field intensity profile, incidence angle and localization at the material surface, the field will propagate along the designed diffraction-compensation axis and preserve its transverse shape and size. In particular, multiple laser beams with coinciding focal spots, but different incidence angles will propagate along the same path in the material, which implies an increased information-transfer capacity of the material compared to conventional waveguides [24]. Furthermore, the material can be used to create wide-angle antireflection and high-reflection coatings or beam splitters acting independently of the incidence angle. The designed metamaterial can also be used in laser technology to create, e.g., planar laser resonators insensitive to the mirror alignment and Fabry-Perot-type intracavity filters free of the wave walk-off problem [25, 26].

#260019 Received 25 Feb 2016; revised 4 Apr 2016; accepted 22 Apr 2016; published 27 Apr 2016

2. Design and characterization of metamaterials

The metamaterials designed in this work consist of a lattice of silver metamolecules embedded in glass. They are conveniently characterized by using the effective refractive index (n) and impedance (Z) seen by a plane wave (fundamental Bloch mode [27, 28]) in the material. Due to spatial dispersion, these parameters depend on the wave propagation direction. The retrieval of n and Z is done by considering reflection and transmission of plane waves by a metamaterial slab [29–31]. If the material contains tilted metamolecules, one has to calculate the slab reflection and transmission coefficients ρ_1 and τ_1 for a wave incident at an angle θ_{i}, and coefficients ρ_2 and τ_2 for a wave incident from the opposite side at an angle $\pi - \theta_{\mathrm{i}}$ [29]. To minimize the computational load, we use a metamaterial with negligible evanescent-wave coupling between the metamolecular layers, in which case the consideration of a single-layer slab is sufficient. In the calculations, the slab is assumed to be surrounded by the host medium. We use the COMSOL Multiphysics software to calculate the field distributions around and inside the slab, which yields the required reflection and transmission coefficients. The normal component of the effective propagation constant in the metamaterial is calculated as

$$k_z = -\frac{\mathrm{i}}{\Lambda_z} \log \left[\frac{\alpha}{2\beta} \pm \left(\frac{\alpha^2}{4\beta^2} - \frac{1}{\beta} \right)^{1/2} \right] + \frac{2\pi m}{\Lambda_z}, \tag{1}$$

where

$$\alpha = f_2 + f_1^{-1}(1 - g_1 g_2), \tag{2}$$

$$\beta = f_2 / f_1. \tag{3}$$

Here, the phase-shifted coefficients $g_i = \rho_i \exp(\mathrm{i}k_{0z}\Lambda_z)$ and $f_i = \tau_i \exp(\mathrm{i}k_{0z}\Lambda_z)$ are used; $\mathbf{k}_0$ is the wave vector in the host medium. The lattice period in the z-direction is denoted by Λ_z and m is a physically justified integer number [29–31]. The refractive index can then be solved from

$$k_{\mathrm{vac}}^2 n^2 = k_{0x}^2 + k_{0y}^2 + k_z^2, \tag{4}$$

where k_{vac} is the wavenumber in vacuum. The impedance is defined as the ratio of the spatially averaged transverse electric and magnetic fields. It is given by

$$Z = Z_0 \left(\frac{k_0 k_z}{k_{0z} k} \right)^{\sigma} \frac{g_2 + [1 - f_1 \exp(-\mathrm{i}k_z\Lambda_z)]}{g_2 - [1 - f_1 \exp(-\mathrm{i}k_z\Lambda_z)]}, \tag{5}$$

where Z_0 is the impedance of the host medium and $\sigma = \pm 1$ for TE- and TM-polarizations, respectively. In general, impedances seen by two counter-propagating waves are equal if the metamaterial is not bifacial [30, 32]. The parameters n and Z are functions of the angle θ_{i} that is connected to the propagation angle θ in the medium by complex Snell's law [33].

The design of diffraction-compensating metamaterials follows the procedure proposed in [22] with the aim to reach suppressed diffraction for three-dimensional optical beams. The procedure allows us to achieve not only three-dimensional diffraction compensation, but also impedance-matching of the metamaterial to the surrounding medium. Then, to model propagation of *optical beams* in the designed metamaterial, we use a general method we have previously developed [34]. The method makes use of a rigorous vectorial plane-wave decomposition that allows one to model the beam-metamaterial interaction very efficiently independently of the beam propagation distance.

The diffraction compensation is achieved when the refractive index plotted in spherical coordinates as a function of the wave propagation direction shows a large enough flat part. We

#260019
Received 25 Feb 2016; revised 4 Apr 2016; accepted 22 Apr 2016; published 27 Apr 2016

fulfill this requirement for TM-polarized waves using a strongly optically anisotropic and spatially dispersive metamaterial composed of silver nanobars in glass. Hence, the material ensures effective diffraction cancellation for optical beams composed of TM-polarized waves, such as radially polarized Hermite-Gaussian modes [35].

3. A diffraction-compensating metamaterial

The metamaterial we have designed has a periodic three-dimensional structure shown in Fig. 1. It consists of silver nanobars arranged in a tetragonal lattice in glass. The nanobars are cuboids with dimensions $L_x = L_y = 30$ nm and $L_z = 130$ nm. The lattice dimensions are $\Lambda_x = \Lambda_y = 120$ nm and $\Lambda_z = 200$ nm. The material is designed to suppress divergence of optical beams propagating along the z-axis. The parameters n and Z were evaluated using Eqs. (4) and (5) for each given angle θ, wavelength and both TM and TE polarizations. For TM-polarized plane waves, the coupling to the longitudinal plasmon resonance of the nanobars is more efficient at larger propagation angles (θ), which leads to a higher refractive index. The unit-cell dimensions are adjusted such that, when plotted in spherical coordinates, the real part of the refractive index forms a flat surface at around $\theta = 0$ and obeys the relation $n(\theta) = n(0)/\cos(\theta)$. The symmetry of the structure makes the refractive index independent of the azimuthal propagation angle, as long as the wave stays TM- or TE-polarized. The same holds for the wave impedance. Hence, to describe the material, it is enough to show only two-dimensional polar plots of $n(\theta)$ and $Z(\theta)$. Figure 2(a) shows these plots for TM-polarized waves at a vacuum wavelength $\lambda_{\text{vac}} = 913$ nm. In the calculations, the spectrum of the refractive index of silver was taken from [36].

The black solid and red dashed curves in Fig. 2(a) show the real and imaginary parts of the wave parameters, respectively. The real part of the refractive index is seen to be flat at small angles θ. The real part of the normalized impedance is close to 1 at these angles, which ensures a low reflection loss at the glass-metamaterial interface. The angles θ corresponding to the gray sectors cannot be reached from glass that has a lower refractive index compared to

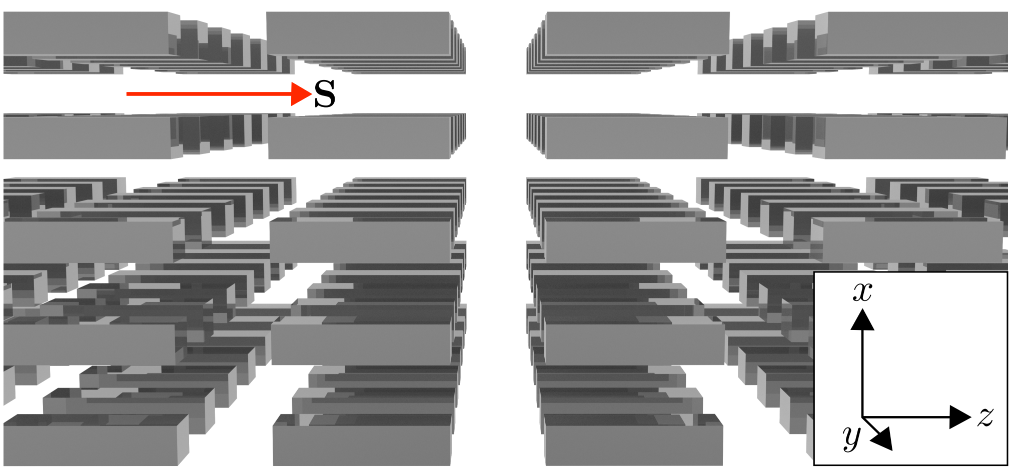

Fig. 1. Diffraction-compensating silver-nanobar metamaterial. The nanobars are 30 nm thick in the x- and y-directions and 130 nm long. They form a tetragonal lattice in glass and suppress optical diffraction for light propagating along the Poynting vector **S**. The unit-cell dimensions are $\Lambda_x = \Lambda_y = 120$ nm and $\Lambda_z = 200$ nm.

#260019 Received 25 Feb 2016; revised 4 Apr 2016; accepted 22 Apr 2016; published 27 Apr 2016

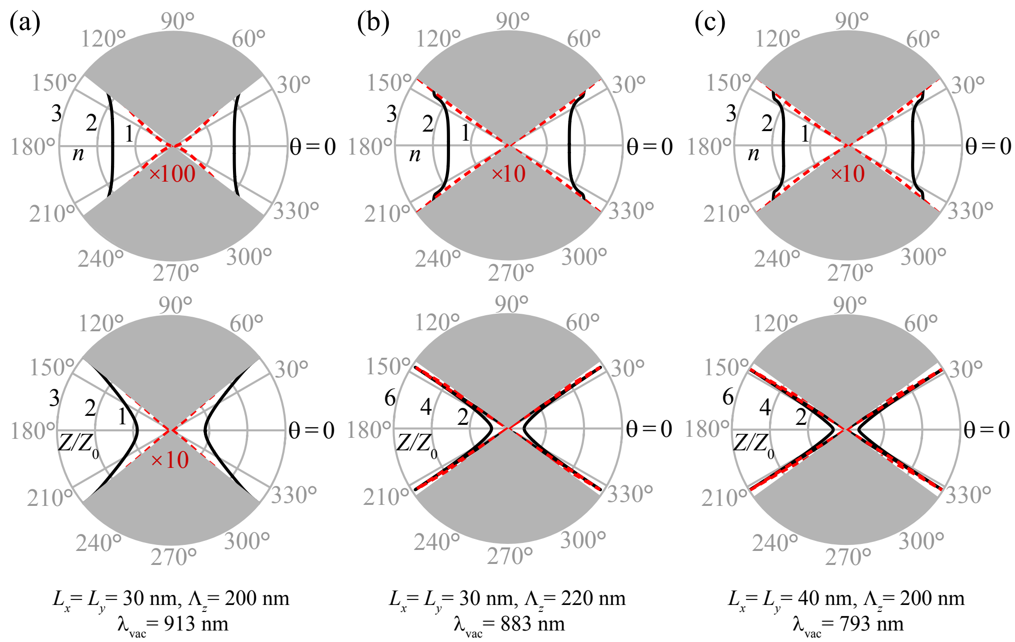

Fig. 2. Refractive index n and normalized impedance Z/Z_0, where Z_0 is the impedance of glass, plotted in polar coordinates as functions of the plane-wave propagation angle θ for three different metamaterials. The black solid and red dashed curves represent the real and imaginary parts of the quantities, respectively. The imaginary parts are multiplied by factors of 100 and 10 as shown for each plot separately. The angles unavailable for waves incident from glass are marked by the gray sectors. The parameter values by which the materials in (a), (b) and (c) differ from each other are as follows: (a) $L_x = L_y = 30$ nm, $\Lambda_z = 200$ nm and $\lambda_{\text{vac}} = 913$ nm, (b) $L_x = L_y = 30$ nm, $\Lambda_z = 220$ nm and $\lambda_{\text{vac}} = 883$ nm, and (c) $L_x = L_y = 40$ nm, $\Lambda_z = 200$ nm and $\lambda_{\text{vac}} = 793$ nm.

the metamaterial. Because the values of $\text{Im}(n)$ and $\text{Im}(Z/Z_0)$ are very small, they have been multiplied by factors of 100 and 10, respectively, in order to make the corresponding curves visible in the pictures [$\text{Im}(n) = 0.0003$ and $\text{Im}(Z/Z_0) = -0.0004$ at $\theta = 0$]. Low values of the absorption and reflection coefficients of the metamaterial are important for good optical-image transfer, since absorption and reflection can significantly reduce the intensity as well as distort the image. A rapid increase of the imaginary part of n and both the real and imaginary parts of Z when θ approaches its maximum value are caused by enhanced excitation of localized surface plasmons and increased spatial dispersion as the structure gets closer to the Bragg-reflection regime when $\text{Re}(n)$ increases.

The difference of the designed metamaterial from a hyperbolic-type metamaterial made of infinitely long wires is in the presence of gaps between the ends of the nanobars. For comparison, we removed these gaps and tried to satisfy the diffraction-compensation and impedance-matching conditions for $\lambda_{\text{vac}} < 1$ μm. The wave parameters were retrieved from numerically calculated reflection and transmission coefficients of a 1 μm thick metamaterial slab. We have verified that the calculated wave parameters are valid also for thicker slabs. The best result was obtained at a slightly longer wavelength of 1.12 μm for a metamaterial with $\Lambda_x = \Lambda_y = 180$ nm ($L_x = L_y = 30$ nm). This hyperbolic-type metamaterial, however, has significant drawbacks compared to the nanobar metamaterial. While at normal incidence it performs very well, the optical absorption and impedance mismatch of the material increase with θ much faster, i.e.,

#260019 Received 25 Feb 2016; revised 4 Apr 2016; accepted 22 Apr 2016; published 27 Apr 2016

when θ increases from 0 to 7°, Im(n) increases from 0.0001 to 0.02 and Z/Z_0 changes from about 0.97 to $0.56-0.07$i. Furthermore, the range of angles for which $n(\theta)$ stays approximately flat is more than three times narrower, being limited by $\theta = 7°$. In addition, within this range the first-order divergence parameter, calculated as the angle-averaged root-mean-square value of the derivative $\partial\text{Re}(k_z)/\partial\text{Re}(k_x)$, is much higher than that of the nanobar metamaterial, 0.07 instead of 0.001. At a fixed θ, this derivative can be considered as the plane-wave inclination parameter [20]. Finally, the wavelength range of the diffraction-compensation regime at small θ is fifty times narrower than for the nanobar metamaterial. This spectral range is defined by requiring that the deviation of $n(\theta)$ from a perfectly flat profile $n_{\text{fl}}(\theta)$ at $\theta = 7°$ stays below $|n_{\text{fl}}(\theta) - n(0)|/10$ – at the limit, it is 10 times smaller than in pure glass. The diffraction-compensation bandwidth of the nanobar material, ca. 50 nm, is relatively wide, which is an important advantage of our metamaterial in view of practical realization of the metamaterial concept and verification of the predicted diffraction-compensation phenomenon.

The wavelength at which the metamaterial is designed to suppress optical diffraction can be changed by tuning some of the structural dimensions. For example, if the longitudinal period Λ_z is changed from 200 nm to 220 nm, the wavelength of the diffraction compensation effect moves from $\lambda_{\text{vac}} = 913$ nm to $\lambda_{\text{vac}} = 883$ nm. The plots of $n(\theta)$ and $Z(\theta)/Z_0$ corresponding to this case are presented in Fig. 2(b). If instead of Λ_z, we change the thickness of the bars, e.g., from 30 nm to 40 nm, the operation wavelength of the material shifts to 793 nm. The functions $n(\theta)$ and $Z(\theta)/Z_0$ calculated for this case are plotted in Fig. 2(c). The refractive-index flatness condition, $n(\theta) = n(0)/\cos(\theta)$, is not anymore strictly satisfied around $\theta = 0$, but met at a larger angle of about 20°. Therefore, the material is expected to provide diffraction compensation for optical images with wider angular spectra (smaller features), but over a shorter propagation distance compared to the materials of Figs. 2(a) and 2(b).

The isofrequency surfaces of the wave parameters evaluated for TE-polarized plane waves are spherical, since essentially, these waves do not interact with the nanobars and "see" only the host medium. The values of the refractive index and impedance for all possible propagation directions of these waves are equal to the corresponding values obtained for TM-polarized waves at $\theta = 0$. Because of this we do not show the plots of $n(\theta)$ and $Z(\theta)$ for the TE-polarization.

4. Propagation of light in the designed metamaterials

To verify the effect of diffraction compensation for light composed of TM-polarized waves, we consider a radially polarized hollow beam at $\lambda_{\text{vac}} = 913$ nm normally incident onto the surface of the metamaterial of Fig. 2(a) from glass. The beam waist is located at the surface and has a radius of 1 µm. In glass, the divergence angle of the beam is 16°. Figure 3(a) shows the longitudinal cross-section of the beam intensity normalized to its peak value. The glass-metamaterial interface is shown by the vertical white line. The beam is seen to propagate in the material essentially free of diffraction over a distance of 50 µm. The reflection loss at the interface is negligibly low (ca. 0.2 %), as expected, since $Z \approx Z_0$ for $\theta < 16°$. The $1/e^2$ power decay length of the beam is evaluated to be ca. 200 µm. To better illustrate the evolution of the beam cross section upon propagation, we show the calculated transverse intensity profiles of the beam at z equal to 100 µm, 200 µm and 300 µm (see Fig. 3(b)). In spite of some divergence of the beam, the diffraction-compensation effect is evident. If, for example, the metamaterial was replaced with glass, the beam radius would at $z = 300$ µm be about 90 µm instead of the observed 1.5 µm. Optical absorption does not affect the shape of the profile, even though the plane-wave absorption coefficient depends on θ. In conclusion, the designed metamaterial shows excellent diffraction-compensation characteristics for radially polarized optical beams. It can be used not only for the considered hollow beam, but also for higher-order Hermite-Gaussian modes with radial polarization.

#260019 Received 25 Feb 2016; revised 4 Apr 2016; accepted 22 Apr 2016; published 27 Apr 2016

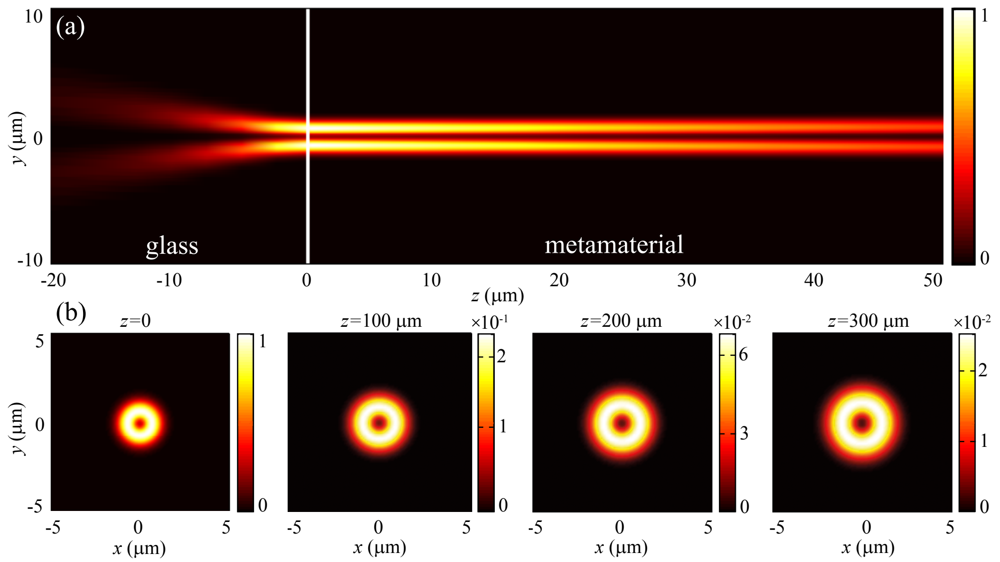

Fig. 3. The longitudinal (a) and transverse (b) intensity profiles of a radially polarized hollow optical beam at $\lambda_{\mathrm{vac}} = 913$ nm focused onto the surface of a diffraction-compensating metamaterial (white line). The cross sections in (b) correspond to the coordinates z of 0, 100 μm, 200 μm and 300 μm. The intensity is normalized to its maximum value at $z = 0$.

In the next step we show that the designed metamaterial can be used to guide not only circularly symmetric, but essentially arbitrary optical images over long distances in the material without distortion. As the material is sensitive to light polarization we choose to use unpolarized radiation to form the original image at the entrance surface of the material. In the calculations, we model unpolarized field by incoherently summing two waves with opposite circular polarizations. Alternatively, one could use orthogonal linear polarizations. Circular polarization, however, includes all possible directions of the transverse electric-field vectors, and in principle, if the image is circularly polarized, it also preserves the shape upon propagation. For images formed by unpolarized light, the intensity is calculated as a sum of the intensities of two orthogonal circularly polarized components.

Figure 4(a) shows the image of the letter M at the entrance surface of the material (at $z = 0$; the material corresponds to that in Fig. 2(a)) and the intensity profiles of the field at a distance of $\frac{1}{3}$ mm, $\frac{2}{3}$ mm and 1 mm from the surface. At the input surface, the field within the M has a planar wavefront and a gradually decreasing intensity at the edges. The edges are made smooth in order to keep the angular spectrum of the incident field within the angular spread of the flat part of $n(\theta)$. The image is seen to preserve its shape even after a 1-mm propagation distance in the material. If the material was replaced with glass, the thickness of each line in the M would at $z = 1$ mm be huge, about 200 μm, making the image absolutely unrecognizable. The optical power confined within the image decreases a bit faster upon propagation than the power of the previously considered radially polarized beam, because the contribution of the TE-polarized plane-wave components to the image vanishes at long propagation distances. Nevertheless, the material clearly exhibits the ability to transfer optical images of any shapes without significant distortions. If instead of unpolarized, circularly polarized light is used, the image starts to show some spiral artefacts visible in Fig. 4(b). Otherwise the image propagates in a similar way with the originally unpolarized image. Two-dimensional images have been previously transfered through metamaterial structures made of effectively infinite metal rods [14], but only over very

#260019 Received 25 Feb 2016; revised 4 Apr 2016; accepted 22 Apr 2016; published 27 Apr 2016

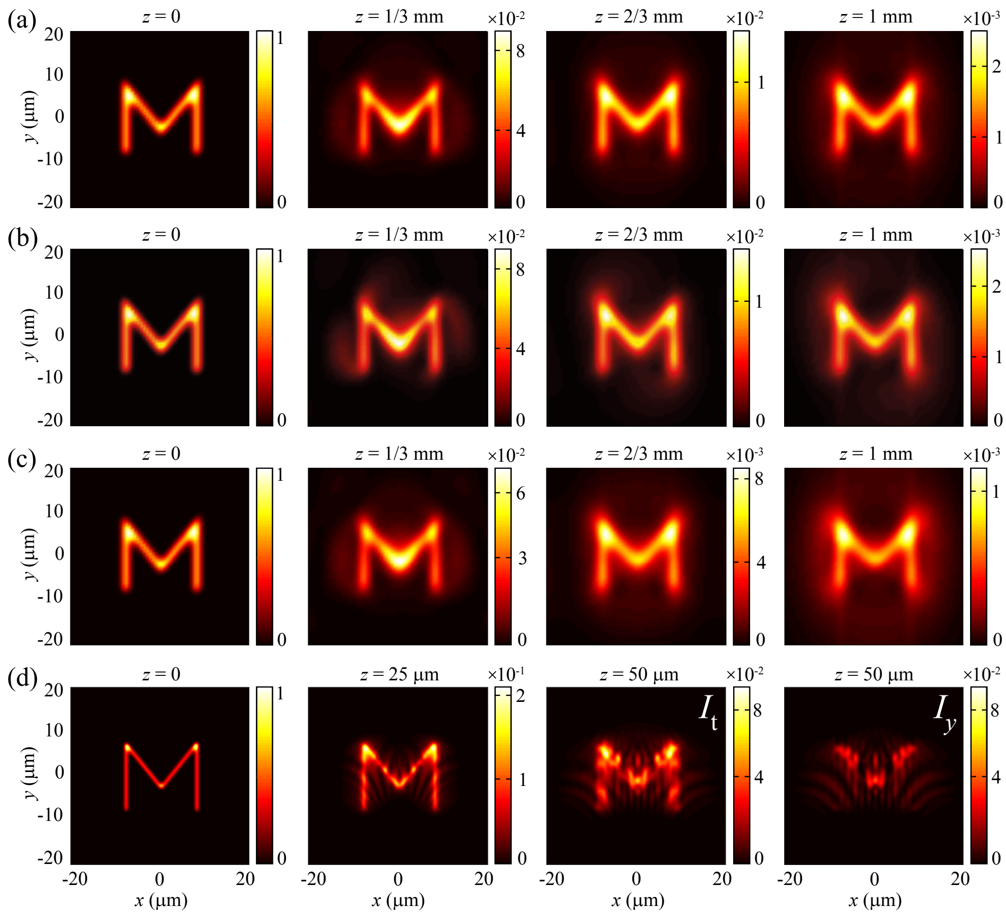

Fig. 4. Propagation of an optical image of letter M in three different diffraction-compensating metamaterials. The z-coordinates of the presented intensity profiles are shown above each profile. The intensity is normalized to its maximum value at $z = 0$. In (a) and (b), the material corresponds to that in Fig. 2(a) and the image is originally formed by (a) unpolarized and (b) left-handed circularly polarized light. In (c), the material corresponds to that in Fig. 2(b) and the image is originally unpolarized. In (d), the material is as in Fig. 2(c) and the image is unpolarized. The two last pictures of case (d) show the total intensity (I_t) and the intensity of the y-polarized part of the image (I_y) at the same coordinate $z = 50$ μm.

short distances, on the order of 10 μm, due to high absorption losses. In our metamaterial design, the absorption is remarkably low.

For the metamaterial adjusted to operate at $\lambda_{\text{vac}} = 883$ nm, the image transfer characteristics are illustrated in Fig. 4(c). A weak halo around the M at $z = 1$ mm is explained by a larger curvature of the refractive-index surface of the TM-polarized waves in this case compared to the case of Fig. 4(a). It is noticeable that, when the originally unpolarized image propagates through the material, it becomes more and more polarized because of the diffraction loss of the TE-polarized components. We have found that after a long enough propagation distance, the image becomes composed of the TM-polarized plane waves only, which does not cause any considerable changes in the details of the image. Hence, the metamaterial acts as a polarizer,

#260019 Received 25 Feb 2016; revised 4 Apr 2016; accepted 22 Apr 2016; published 27 Apr 2016

but in a conceptually new way, making the field be composed of TM-polarized waves.

The propagation-induced gain of the degree of polarization within the image is illustrated in Fig. 4(d). We choose the metamaterial of Fig. 2(c) - as it has a wider flat part of $n(\theta)$ - and make the lines composing the M thinner to increase the divergence of its TE-polarized part. The width of the lines is now only 400 nm, while the wavelength is 793 nm. The intensity profiles of the image are shown for the propagation distances of 25 μm and 50 μm. The two last intensity profiles in Fig. 4(d) correspond to the same propagation distance of 50 μm, but in the first picture we show the total intensity (I_t), while in the second one, only its y-polarized component (I_y). We see that the image is polarized mostly in the direction perpendicular to the lines of the M, which proves that the image is composed of the TM-polarized waves. The major distortion of the image is in the appearance of a double-slit-type interference pattern. This pattern originates from a non-negligible curvature of the $n(\theta)$-contour and a stronger divergence of light due to narrower features of the image.

5. Conclusions

In this paper, we have introduced a simple metamaterial design that provides compensation of optical diffraction for radially polarized optical beams. In addition, we have demonstrated nearly propagation-invariant transfer of essentially arbitrary two-dimensional images created by unpolarized or circularly polarized waves. The wave impedance and the operation wavelength of the material were adjusted by tuning the dimensions of the nanobars and the unit cells. The metamaterial was designed to be approximately impedance-matched to glass in order to minimize the reflection loss at the glass-metamaterial interface.

In the material, images composed of TE-polarized waves diverge as fast as in glass. Therefore, initially unpolarized intensity profiles preserve their shapes and become polarized (composed of TM-polarized waves) upon popagation in the material. Hence, the material acts as a new type of an optical polarizer. We foresee applications of the designed metamaterial in optical imaging systems, integrated optics, optical communications, and in microfabricated light sources and detectors. We believe that in the future, diffraction-compensating metamaterials can be further developed to obtain even lower optical absorption loss and higher-quality image transfer.

Acknowledgments

V. K. acknowledges financial support from the Vilho, Yrjö and Kalle Väisälä Foundation of the Finnish Academy of Science and Letters.